$\Delta\mathrm{PSD}(f) = \mathrm{PSD}(f)/\sqrt{N_b(f)}$ standard deviation for the logarithmically spaced points in the frequency range. At the same time, a uniform binning, corresponding to a uniform relative error was assigned to the MSD and the VAF, chosen arbitrarily to be 10%: $\Delta\mathrm{MSD}(t) = 0.1 * \mathrm{MSD}(t)$, $\Delta\mathrm{VAF}(t) = 0.1 * \mathrm{VAF}(t)$. The input parameters for the synthetic data were the following:

$$R_\mathrm{p} = 0.7\ \mu\mathrm{m}$$
$$K = 15\ \mu\mathrm{N/m}$$
$$\beta^2 = 1700\ \mathrm{nm}^2/\mathrm{V}^2$$
$$\mathrm{PSD}_\mathrm{rot} = 0.008\ \mathrm{V}^2/\mathrm{Hz}$$
$$\mathrm{MSD}_\mathrm{rot} = 0.36\ \mathrm{V}^2$$

The last two parameters were used for the simulation the additional rotational fluctuations (14), (15), (16). We applied the physical properties of silica and water at $T = 22°\mathrm{C}$ to simulate experimental conditions identical to the real measurements described in the following section: $\rho_\mathrm{p} = 1.96\ \mathrm{g/cm}^3$, $\rho_\mathrm{f} = 0.997\ \mathrm{g/cm}^3$, $\eta_\mathrm{f} = 0.955\ \mathrm{mPas}$.

100 datasets were generated with the same input parameters but random additional noise. All datasets were fitted by each fitting option to test the distribution of the fitted parameters (shown in Figure 5). The best performance was achieved in the linear option, where the functions and input data were left untransformed, and were weighted by the error values. The fitted parameters scatter around the real values and the obtained 95% confidence intervals predict well the actual standard deviation of the results (confidence intervals not shown). In case of the logarithmic transformation without weighting, the fitting converges to multiple discrete points around the real value (red histogram), which implies that new local minima are introduced by the nonlinear transformation. Using the global minimum search option (blue histogram) highly improves the results. The parameter estimates are not biased, though the standard deviation of the fitted values is somewhat larger than that in the linear mode. The advantage of the logarithmic transformation is that the fitting can converge without weighting, which makes it possible to fit data even when no errors were previously estimated. All other fitted parameters follow similar distributions and are thus not shown here.

8.2. Test results on measured data

Test measurements were performed with custom-made optical tweezers [13] utilizing a diode-pumped Gaussian beam, ultra-low noise Nd:YAG laser with a wavelength of $\lambda = 1064\ \mathrm{nm}$, and a maximal light power of 500 mW in continuous wave mode (IRCL-500-1064-S, CrystaLaser, USA). The trapping light was focused by a high numerical aperture (NA=1.2), 60x water-immersion objective (UPLapo/IR,Olympus, Japan). The position detection was achieved by an InGaAs quadrant photodiode with an active area of 2 mm in diameter (QPD,

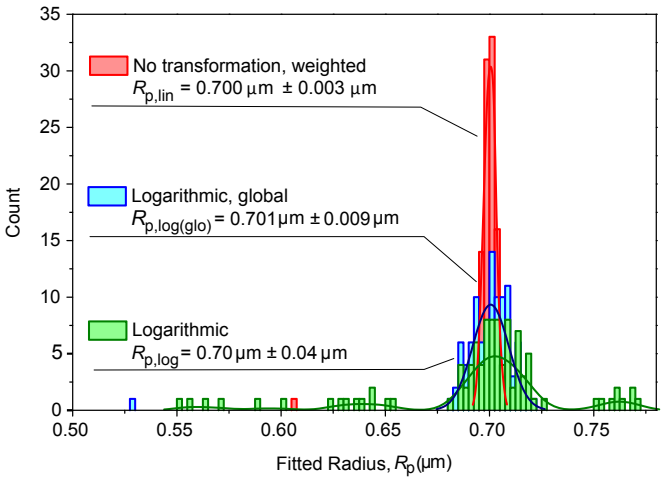

Figure 5: Distribution of the fitted radius, R_{p}, for synthetic data using three different fitting options. Red, green and blue colors represent 'Linear', 'Logarithmic' and 'Logarithmic' along with 'Global minimum' options respectively. The fitted curves on the top of the histograms are guides to the eye. The real radius was $R_{\mathrm{p}} = 0.7\,\mu\mathrm{m}$. The mean and the standard deviation of the 100 fittings are summarized in the legend for each option.

G6849, Hamamatsu Photonics, Japan). Data were collected by a data acquisition board with a dynamic range of 12 bits (NI-6110, National Instruments, USA) at 1MHz sampling rate. The cutoff of the amplification system at the maximal gain of 500 was around 1 MHz. The $\mathrm{PSD}^{\mathrm{exp}}$, $\mathrm{MSD}^{\mathrm{exp}}$ and $\mathrm{VAF}^{\mathrm{exp}}$ data were calculated by a custom-designed program.

Silica spheres were used to test the 'Spherical' fitting option (Figure 6 (d)). The bead radius is known from the manufacturer to be 0.505 µm within 4% tolerance. The physical parameters were the following: $\rho_{\mathrm{p}} = 1.96\,\mathrm{g/cm^3}$, $\rho_{\mathrm{f}} = 0.997\,\mathrm{g/cm^3}$, $\eta_{\mathrm{f}} = 0.955$ mPas, the measurement was performed at $T = 22^{\circ}\mathrm{C}$. The low-frequency noise was cropped by setting the fitting range to $5\mathrm{Hz} - 10^6\mathrm{Hz}$. The obtained parameters in the different fitting modes are summarized in (Table 7).

Opting for no logarithmic transformation of the data now provides inconsistent results. The fitted radius in the linear mode is: $R_{\mathrm{p}} = 0.34 \pm 0.01\,\mu\mathrm{m}$, which differs significantly from the real radius of the probe, whereas the logarithmic mode returns the correct value: $R_{\mathrm{p}} = 0.52 \pm 0.02\,\mu\mathrm{m}$. Despite the large discrepancy between the two sets of fitted parameters, the PSD and MSD curves are fitted with apparently the same quality, allowing no distinction between the two results (Figure 6 (a) and (b)). Fitting the VAF function on the other hand, which is very sensitive to the bead size in the short time limits, clearly reveals the discrepancy (Figure 6 (c)).

In order to investigate the Brownian motion of a randomly shaped object, larger silica spheres of 100 µm diameter were crushed in a mortar to $1 - 2$ µm

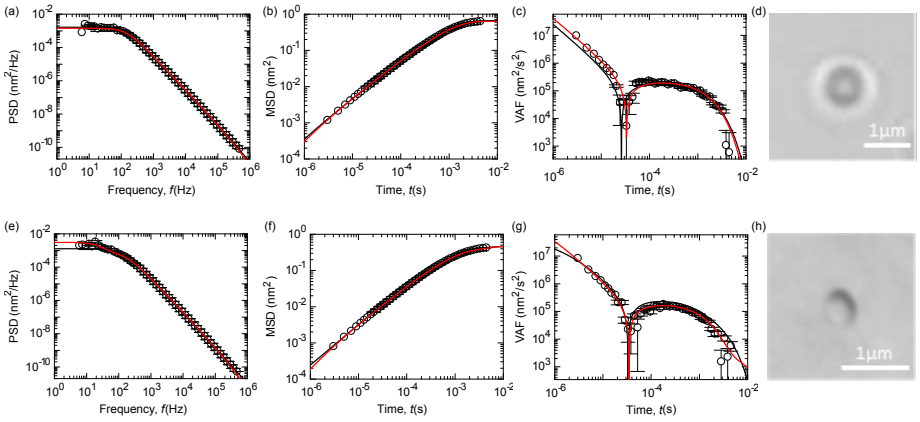

Figure 6: Fitting results for the PSD MSD and VAF experimental data measured on a $R_{\mathrm{p}} = 0.505$ μm diameter silica sphere captured in the trap (top row, (a)-(c)), as well as on a non-spherical silica probe (bottom row, (e)-(g)). Black circles indicate experimental points. Black fitted curves were obtained using the 'Linear fitting' option, whereas red curves show the result of fitting with 'Logarithmic transformation' option. CCD camera images of the captured probes are displayed in the fourth column (d), (h). White bars indicate 1 μm length.

randomly sized particles, one of which was captured by the optical trap (Figure 6 (h)). The occurrence of a second plateau can be seen in the PSD (Figure 6 (e)) and can be readily fitted by the non-spherical model. Again, low-frequency noise below 5 Hz has been cropped. As in the previous case, the logarithmic transformation provides the better fitting results (Table 7).

The cause of the ill-convergence for the untransformed data might be the poor estimation of the error values, which introduces a bias to the weighting. The restoring force of the optical trap introduces long-time correlations in the trajectory of the probe, which are transmitted to the MSD and VAF functions at long lag times. Since the number of independent data points in each bin are reduced, the errors are systematically underestimated. A possible way to overcome this problem is given by Flybjerg and Petersen in [6].

We performed again the fitting within a constrained range of $t = 10^{-6} - 10^{-3}$ s. Furthermore, to avoid aliasing effects at frequencies near the sampling frequency, the fitting limits have been set to $f = 5\,\mathrm{Hz} - 10^5\,\mathrm{Hz}$ in the frequency range. As shown in Table 7, the fitting in the linear mode now yields consistent results.

In order to demonstrate the robustness of the methodology, the automated fitting procedure has been executed using experimental data from a series of consecutive measurements on a single polystyrene sphere in the optical trap. The nominal radius of the bead was 0.74 μm with a density of $\rho_{\mathrm{p}} = 1.05\,\mathrm{g/cm^3}$. The polarization direction of the trapping laser was rotated by 20° with a half-wave plate between each measurement up to more than one and a half full cycle (560°). Fitting ranges were set to $t = 10^{-6} - 10^{-3}$s and $f = 100\mathrm{Hz} - 10^5\,\mathrm{Hz}$. Figure 8 displays the fitting results for all polarization angles, ϕ. The radius of the

Probe	Mode	Range f(Hz)	Range t(s)	R_p (μm)	k (μN/m)	β^2 (nm²/V²)
Spherical	Lin	5-10⁶	10⁻⁶-10⁻²	0.34 ± 0.01	4.82 ± 0.2	2560 ± 102.7
	Lin	5-10⁵	10⁻⁶-10⁻³	0.5 ± 0.005	8.22 ± 0.17	1640 ± 25
	Log	5-10⁶	10⁻⁶-10⁻²	0.52 ± 0.02	8.4 ± 0.6	1528 ± 70
Non-spherical	Lin	5-10⁶	10⁻⁶-10⁻²	1.62 ± 0.06	57.2 ± 4.2	1332 ± 65.5
	Lin	5-10⁵	10⁻⁶-10⁻³	0.73 ± 0.03	17.19 ± 1.12	1746 ± 23.8
	Log	5-10⁶	10⁻⁶-10⁻²	0.71 ± 0.03	15.0 ± 1.4	1684 ± 70.3

Figure 7: Comparison of the fitting parameters obtained for a spherical silica bead as well as a non-spherical silica particle using different fitting options.

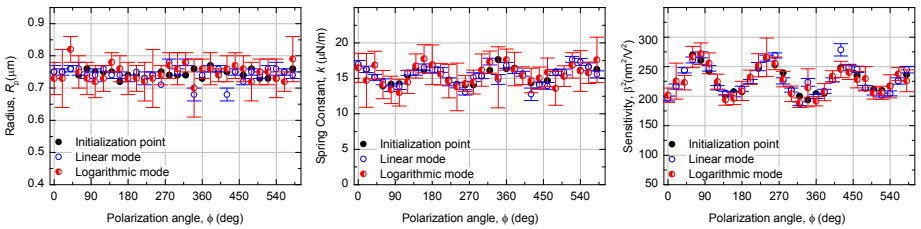

Figure 8: Obtained fitting parameters (radius: (a), spring constant: (b) and detector sensitivity: (c)) in the function of the polarization angle of the trapping laser. The initialization points are displayed by black dots. Blue and red dots indicate parameters yielded by the linear and logarithmic fitting mode, respectively. Error bars represent the associated 95% confidence intervals obtained by the fitting algorithm.

bead is estimated accurately both in the linear (blue dots) and the logarithmic mode (red dots). Moreover, the initialization points (black dots) also provide a very good approximation of the real radius, meaning that the characteristic points of the MSD and VAF curves - which define the initial parameters - can be measured and determined with high accuracy. Whereas the 95% confidence intervals in the logarithmic mode agree well with the distribution of the fitted points, in the linear mode there are more outliers than statistically expected. This suggests that the confidence intervals are somewhat underestimated by the algorithm, probably due to the underestimation of the error values for some of the experimental data points.

Upon the rotation of the polarization of the trapping light, the obtained spring constant and sensitivity values (Fig. 8(b) and (c)) are periodically modulated with a periodicity of 180°. The modulation of the spring constant originates from the polarization induced asymmetry in the trapping potential. Furthermore, a change in the laser intensity may arise if there is any polarizing elements in the light path, which would cause a modulation of both the spring constant and the detector sensitivity. The fitted parameters show very good consistency and reproducibility, confirming the applicability of the software.

9. Conclusion

We have developed a calibration software for optical tweezers based on the Brownian motion of the probe, sampled with high frequency. In our model we employ the proper hydrodynamic theory for the PSD, MSD and VAF, as well as a qualitative extension for handling rotational fluctuations, or alternatively any additional relaxation processes involved in the dynamics of the particle. The software was tested for synthetic and experimental data. The results confirmed the applicability of the software.

10. Acknowledgment

A.B. was supported by the Hungarian Research Funds, OTKA K 108918. F. M. M. acknowledges support from the National Centre of Competence in Research (NCCR Nano-Bio, Project 1.4) and the Swiss National Science Foundation (SNSF, Project numbers 206021_121396 and 200021_143703). F. M. M. was supported by the National Competence Center in Biomedical Imaging (NCCBI).